RSC Advances

ROYAL SOCIETY OF CHEMISTRY

PAPER

View Article Online
View Journal | View Issue

Check for updates

Cite this: *RSC Adv.*, 2024, **14**, 16704

Efficient optimization of the synthetic conditions for aerosol-assisted high-quality mesoporous CeO_2 powders†

Tatsuo Kimura *

Received 4th March 2024
Accepted 7th May 2024

DOI: 10.1039/d4ra01674b

rsc.li/rsc-advances

The morphology of surfactant-assisted mesoporous metal oxides was tuned to obtain high surface-area particles by utilizing the synthetic conditions for fabricating transparent thin films through an evaporation-induced self-assembly (EISA) process. For investigating their potential applications, especially for designing heterogeneous catalysts, mesoporous metal oxides should be obtained in powder forms; however, a serious limitation associated with their reproducibility persists. Herein, along with a rapid optimization approach, starting from determining and improving chemical composition for the fabrication of mesoporous metal oxide films, an advanced approach to obtain highly porous metal oxide powders is presented using a temperature-controlled spray-drying process with step-by-step but smooth optimization by combining several EISA processes, involving the utilization of a precursor solution optimized for a slow-drying process in the case of ceria (CeO_2) using poly(styrene)-*block*-poly(ethylene oxide) (PS-*b*-PEO).

1. Introduction

Ordered mesoporous materials prepared using amphiphilic organic compounds such as alkyltrimethylammonium (C_nTMA) halides, alkyl poly(oxy ethylene) (C_nEO_m), and poly(oxy ethylene)-*block*-poly(oxy propylene)-*block*-poly(oxy ethylene) ($EO_nPO_mEO_n$) have potential for a wide variety of applications owing to the adjustability of mesopores, high exposure of their surfaces, and large capacity of mesopores.[1–5] The morphology of ordered mesoporous materials should be designed for each application, but it is still not easy to tune them on demand in a powder form, which is generally required for the preparation of heterogeneous catalysts. For example, powder samples of mesoporous metal oxides such as alumina (Al_2O_3) have been mainly prepared by applying a room-temperature slow drying process of clear precursor solutions.[6,7] The evaporation-induced self-assembly (EISA) process is vital for synthesizing highly ordered mesoporous metal oxide films using amphiphilic organic compounds[8–10] and is also applicable for obtaining corresponding powders.[11–13] However, the evaporation rate of solvents (*e.g.*, ethanol and water) is not the same during each process of room-temperature spin-coating, temperature-controlled spray-drying, *etc.* Especially, the evaporation rate of such solvents during the room-temperature drying process for recovering metal oxide powders is totally different from those of other processes. The area of an air–liquid interface depends on the size of the container and is important for accelerating the evaporation of solvents, which is strongly influenced by ambient conditions, such as room temperature and humidity. This is often the main concern in the reproducibility of surfactant-assisted mesoporous metal oxides through the drying process.

A wide variety of mesoporous metal oxide powders have thus far been prepared using surfactants by room-temperature slow drying and temperature-controlled fast spray-drying precursor solutions. Both EISA processes need long working times to investigate all the synthetic conditions, including the chemical composition of each precursor solution. From this viewpoint, our approach for obtaining high-quality mesoporous metal oxide powders is quite beneficial for the smooth optimization of synthetic conditions by combining several EISA processes. By utilizing the synthetic conditions for fabricating an ordered mesoporous metal oxide film, the chemical composition of a precursor solution can be determined very quickly *via* a rapid spin-coating process with fast evaporation of solvents. The same precursor solution is then applied to the fast spray-drying process and optimized further for increasing the resultant porosity. According to this realistic approach, we can save much of the working time for optimizing chemical composition, which has already been demonstrated through the synthesis of porous Al_2O_3 powders using poly(styrene)-*block*-poly(ethylene oxide) (PS-*b*-PEO).[14–16]

In this study, this synthetic approach was enhanced further as a useful choice for optimizing the chemical composition of a precursor solution very smoothly for obtaining aerosol-

---

National Institute of Advanced Industrial Science and Technology (AIST), Sakurazaka, Moriyama-ku, Nagoya 463-8560, Japan. E-mail: t-kimura@aist.go.jp

† Electronic supplementary information (ESI) available. See DOI: https://doi.org/10.1039/d4ra01674b

assisted metal oxide powders with surfactant-assisted mesopores. A precursor solution optimized for recovering mesoporous metal oxide powders by the room-temperature drying process with a slow evaporation of solvents was applied for the synthesis of the corresponding films by spin-coating. After finding the molecular structure of PS-*b*-PEO with the best potential for obtaining ordered and/or highly porous films, the corresponding powders were recovered by the spray-drying process (see Scheme 1). This step-by-step but smooth optimization by combining several EISA processes was proved for the synthesis of highly porous ceria (CeO_2) powders in the presence of amphiphilic organic compounds, such as PS-*b*-PEO. This is a significant advance as a time-saving approach to obtain high-quality mesoporous metal oxide powders, which could be potentially started from the chemical compositions found in a huge number of research papers on obtaining room-temperature drying powders of mesoporous metal oxides.

2. Experimental

2.1 Chemicals

Ethanol (99.5%, EtOH), tetrahydrofuran (dehydrated, THF), and cerium(III) nitrate hexahydrate ($Ce(NO_3)_3 \cdot 6H_2O$) were obtained from FUJIFILM Wako Pure Chemical Co. A series of poly(styrene)-*block*-poly(ethylene oxide) (PS-*b*-PEO) materials were purchased from Polymer Source Inc. and utilized as received. According to the analytical data sheets, the molecular structure is expressed by using the molecular weight of PS and PEO units, like 2700-*b*-4000, 10 000-*b*-19 500, 10 000-*b*-21 000, 12 200-*b*-23 900, 16 000-*b*-7500, 16 400-*b*-39 500, 18 000-*b*-7500, 18 000-*b*-39 000, 35 000-*b*-17 000, 40 000-*b*-25 500, 40 000-*b*-31 000, 40 000-*b*-40 500, 40 000-*b*-53 000, 51 000-*b*-28 000, 53 000-*b*-15 000, 58 500-*b*-37 000, 58 600-*b*-71 000, 59 000-*b*-31 000, 59 000-*b*-72 000, 60 000-*b*-18 000, 60 000-*b*-36 000, 60 000-*b*-61 000, 60 000-*b*-85 000, 65 000-*b*-85 000, 65 000-*b*-97 000, 90 000-*b*-45 000, 100 000-*b*-150 000, 105 000-*b*-155 000, 116 000-*b*-164 000, and 125 000-*b*-177 000.

2.2 Synthesis of PS-*b*-PEO templated films and powders of CeO_2

According to the literature for the synthesis of a mesoporous CeO_2 powder sample through a drying process in the presence of a laboratory-made PS-*b*-PEO,[17] a PS-*b*-PEO containing precursor solution was prepared as follows. $Ce(NO_3)_3 \cdot 6H_2O$ (0.30 g) was dissolved in EtOH (7.0 mL), stirred for 60 min, and then mixed with THF (7.0 mL) containing PS-*b*-PEO (0.10 g). The precursor solution was just spin-coated over a UV–ozone-treated clean Si wafer at room temperature (21–22 °C) with ambient humidity (~30%). The resultant CeO_2 film was heated up to 400 °C at a heating rate of 1 °C min^{-1} in a flow of N_2, kept for 1 h under the same conditions, and then calcined for 2 h at that temperature in a flow of O_2. After checking the formation of PS-*b*-PEO-templated mesopores, the precursor solution was spray-dried at 140 °C and the resultant powder sample was calcined at 400 °C in the same manner.

2.3 Characterization

Field-emission scanning electron microscopy (FE-SEM) images were taken using a high-resolution model HITACHI SU9000. For checking the formation of PS-*b*-PEO-templated large-sized mesopores, the resultant powder sample was directly observed (0.7 kV, 10 mA) using a sample folder for retarding the deposition of any conductive metals. Transmission electron microscopy (TEM) images were taken using a JEOL JEM-2010 instrument, operated at 200 kV. Nitrogen (N_2) adsorption–desorption isotherms were measured using an Anton Paar Autosorb-iQ instrument at 77 K after the samples were preheated at 110 °C for 6 h under vacuum. The specific surface areas were calculated by the Brunauer–Emmett–Teller (BET) method using the adsorption data below $P/P_0 = 0.30$. Total pore volumes were estimated using the volume of N_2 at $P/P_0 = 0.99$. X-Ray diffraction (XRD) patterns were recorded using a Rigaku RINT 2100 diffractometer with monochromated Cu Kα radiation (40 kV, 30 mA).

3. Results and discussion

The molecular structure of PS-*b*-PEO helpful for obtaining a highly porous spin-coated film of CeO_2, as utilized with a completely equivalent chemical composition that was applied in a previous innovative paper,[17] was identified by a quick screening of PS-*b*-PEO. In the previous paper, laboratory-made PS-*b*-PEO was utilized for the recovery of dried-up powders and/or a film-like bulk as porous CeO_2 powders.[17] Such a PS-*b*-

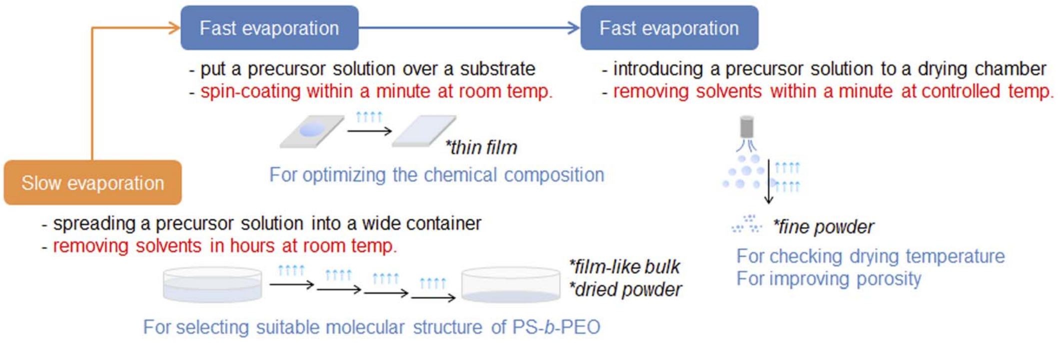

Scheme 1 Schematic summary of the developed process to optimize the synthetic conditions for synthesizing highly porous metal oxide powders using amphiphilic organic compounds by combining several EISA processes.

PEO could not possibly be prepared elsewhere in many cases and it would be better to find commercially available ones suitable for the synthesis of porous CeO_2 powders. Accordingly, the same precursor solutions containing successful PS-*b*-PEO compounds were spray-dried at an appropriate temperature for validating the formation of PS-*b*-PEO-templated pores throughout the resultant CeO_2 powders after calcination. The amount of PS-*b*-PEO was also verified for further increasing the resultant porosity if necessary.

3.1 Highly porous mesoporous CeO_2 films

A wide variety of PS-*b*-PEO diblock copolymers were utilized to fabricate the CeO_2 films by spin-coating (see Fig. S1 and S2†). As provided in Fig. 1, several PS-*b*-PEO molecules, especially 16 000-*b*-7500 and 59 000-*b*-31 000, were found for obtaining high-quality porous CeO_2 films (see (a) and (d) in Fig. 1). The pore diameters after calcination at 400 °C were estimated to be ∼20 nm and ∼35 nm by SEM, respectively. Besides, the molecular structures having PS > PEO (*e.g.*, 35 000-*b*-17 000 and 40 000-*b*-25 500) seemed useful for the formation of spherical pores, but much larger pores could not be structured in resultant films thinner than the pore diameters. Scratched off powders of the CeO_2 films prepared using 16 000-*b*-7500 and 59 000-*b*-31 000 were characterized by TEM (see (b) and (e) in Fig. 1), revealing the presence of large-sized mesopores surrounded by nanoparticles of CeO_2 crystallized to its cubic phase with the space group $Fm\bar{3}m$.[18–21] Interestingly, their particle size was almost homogeneous throughout the mesoporous CeO_2 films, with the average size of around 3 nm (see (c) and (f) in Fig. 1).

In the process of the soft-templating of mesoporous CeO_2 using amphiphilic organic compounds,[22] a hydrogenated poly(butadiene)-*block*-poly(ethylene oxide) (PHB-*b*-PEO, named as KLE, $H[CH_2CH_2CH_2CH(CH_2CH_3)]_n(OCH_2CH_2)_mOH$ with a molecular weight of 4400-*b*-3920 g mol^{-1}) was the most successful one for obtaining an ordered mesoporous CeO_2 film.[18] KLE is one of the famous amphiphilic organic compounds for obtaining a wide variety of metal oxides containing large-sized spherical mesopores.[23] In the case of CeO_2, the formation of large-sized mesopores (14 nm and more) was confirmed by TEM and the mesoporous structure was maintained even after crystallization of the CeO_2 frameworks by calcination at 550 °C.[18] In the synthesis of mesoporous CeO_2 films using Pluronic P123 ($EO_{20}PO_{70}EO_{20}$), which is a commercially available $EO_nPO_mEO_n$ type triblock copolymer, the aging time of the CeO_2 sol, the relative humidity during dip-coating, and the calcination temperature were very important for tuning the size of the CeO_2 nanocrystals that should be accommodated inside the limited space of the thin CeO_2 frameworks around the $EO_nPO_mEO_n$ micelles.[24] Compared to the size of the resultant micelles of the asymmetric KLE and symmetric Pluronic P123, KLE seemed preferable for accommodating large-sized mesopores with the formation of thick CeO_2 frameworks. In this study, the high-molecular-weight PS-*b*-PEO type amphiphilic organic compounds were asymmetric and thus useful for obtaining large-sized mesoporous CeO_2, as in the case of other metal oxides.[18,23,25–28]

3.2 Highly porous mesoporous CeO_2 powders

The same precursor solutions were spray-dried at an inlet temperature at 140 °C and the recovered powders were heated up to 400 °C in a flow of N_2, kept for 1 h under the same conditions, and then calcined at that temperature in a flow of O_2 for 2 h. The SEM image of the calcined sample prepared using 16 000-*b*-7500 (0.10 g) clearly showed the opening of PS-*b*-PEO-templated large-sized mesopores throughout the CeO_2 particles after calcination at 400 °C (see (a) in Fig. 2). The morphology seemed different from that observed for mesoporous metal oxide particles, which were typically aggregated as spherical ones, prepared by an aerosol-assisted synthesis using

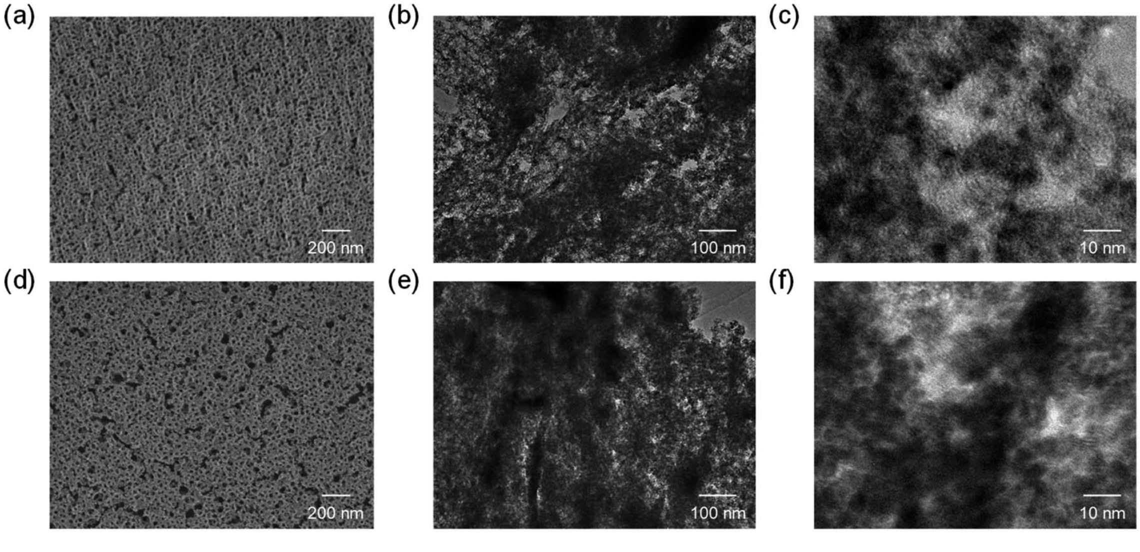

Fig. 1 Surface SEM images of CeO_2 films prepared using (a) 16 000-*b*-7500 and (d) 59 000-*b*-31 000 by spin-coating and subsequent calcination at 400 °C, with (b and c) and (e and f) showing TEM images of their scratched films.

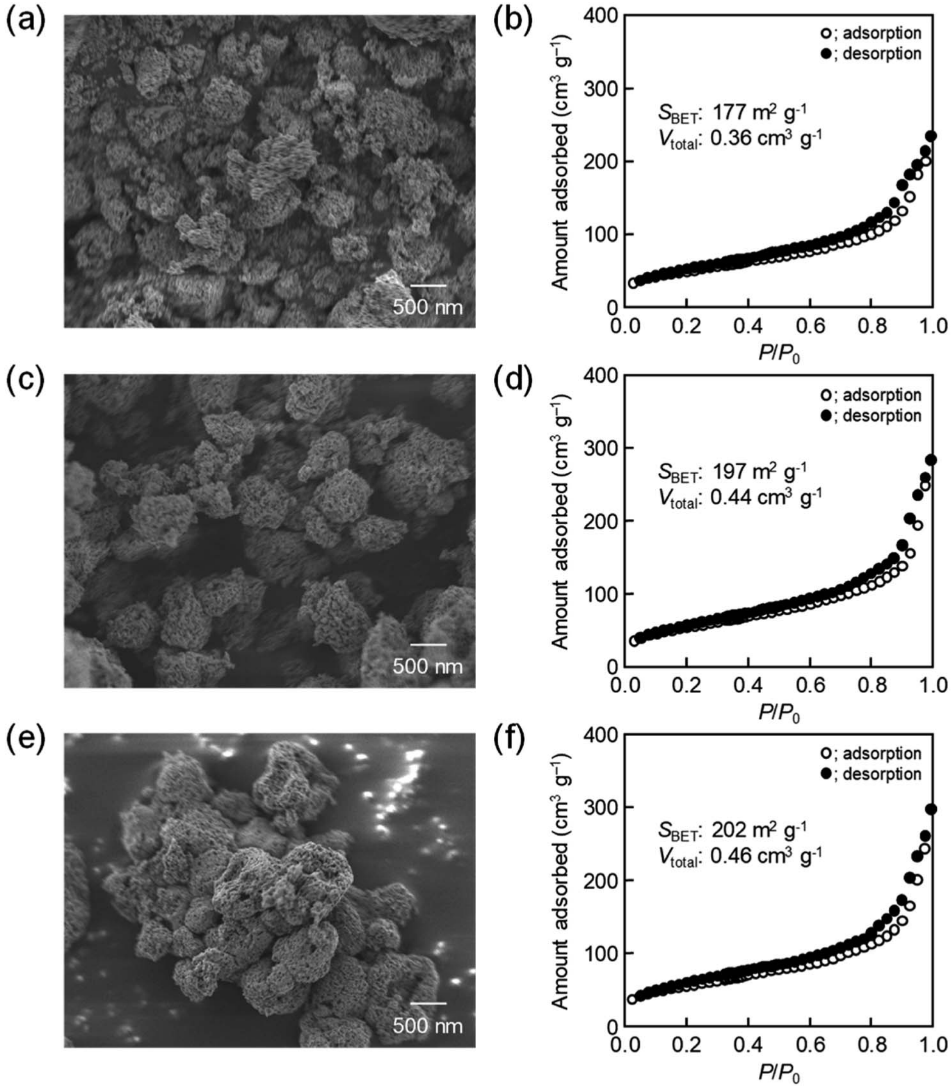

Fig. 2 SEM images of CeO_2 powders prepared using (a) 0.10 g, (c) 0.12 g, and (e) 0.14 g of 16 000-*b*-7500 *via* spray-drying and calcination at 400 °C, with (b, d and f) corresponding N_2 adsorption–desorption isotherms.

amphiphilic organic molecules.[14–16,27] This was likely be due to the strongly ethanolic synthesis without water showing a high surface tension. The TEM images revealed that the PS-*b*-PEO-templated mesopores were surrounded by fine CeO_2 nanoparticles (around 3 nm) (see (a) and (b) in Fig. 3). The N_2 adsorption–desorption isotherm was almost type V (see (b) in Fig. 2) as indicated by the presence of large-sized mesopores.[16,25–27] The BET surface area and the total pore volume were 160 $m^2\ g^{-1}$ and 0.35 $cm^3\ g^{-1}$, respectively.[31] These extremely large values come from the presence of intercrystalline spaces of the resultant fine nanoparticles of CeO_2 in addition to the surfaces of the PS-*b*-PEO-templated mesopores. Some diffraction peaks that could be assigned to the typical cubic $Fm\bar{3}m$ phase of CeO_2 were clearly detected in the wide-angle XRD pattern (see (a) in Fig. 4).

In the early papers on the synthesis of mesoporous CeO_2 samples using Pluronic P123, it was rather difficult to structure ordered mesopores by a drying process.[29,30] Still, the mesoporous structure was stable after calcination below 500 °C (120–150 $m^2\ g^{-1}$ after calcination at 400 °C and 80–110 $m^2\ g^{-1}$ after calcination at 500 °C) even when the CeO_2 frameworks were crystallized to the cubic $Fm\bar{3}m$ phase.[19–21] The mesopores though were deformed and finally collapsed by further crystallization at around 600 °C and the grain growth of CeO_2 nanocrystals at higher temperature.[30] Large-sized mesopores that are surrounded by thick frameworks allow abundant crystallization and the extra phase transformation of metal oxide species.[14–16] The use of preformed CeO_2 nanocrystals (∼3 nm) is a suitable approach for obtaining mesoporous CeO_2 powders using EO_n-$PO_m$$EO_n$ smaller than KLE and PS-*b*-PEO (for example, 160 $m^2\ g^{-1}$ and 0.35 $cm^3\ g^{-1}$ after calcination at 500 °C).[19,21,31] In summary, according to the added benefits of using PS-*b*-PEO, this study was very successful at obtaining highly porous powders structured by highly crystallized CeO_2 nanocrystals.

The amount of 16 000-*b*-7500 was, besides, increased to 0.12 g and 0.14 g for checking the possibility to increase the

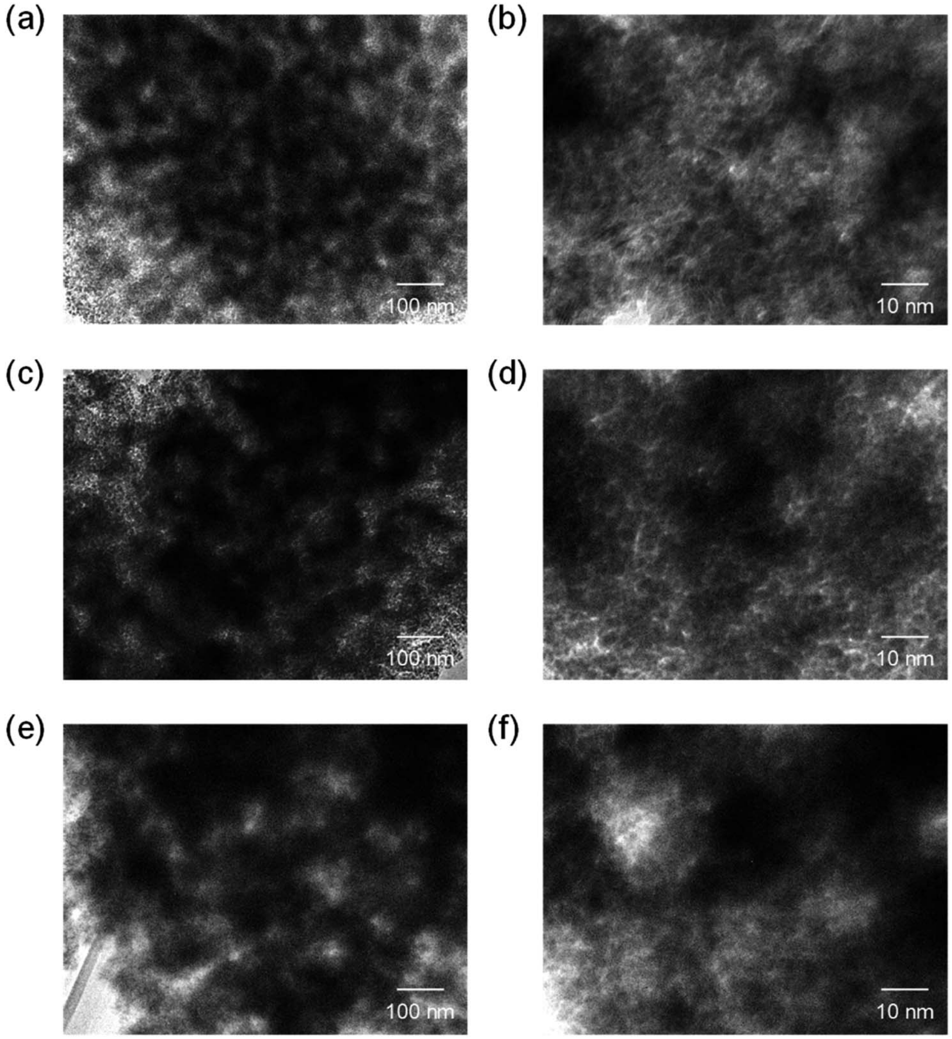

Fig. 3 TEM images of CeO_2 powders prepared using (a and b) 0.10 g, (c and d) 0.12 g, and (e and f) 0.14 g of 16 000-*b*-7500 *via* spray-drying and calcination at 400 °C.

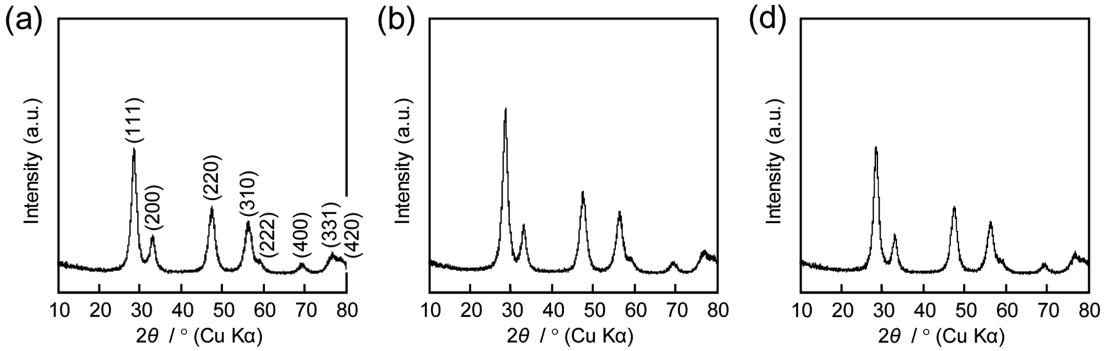

Fig. 4 XRD patterns of CeO_2 powders prepared using (a) 0.10 g, (b) 0.12 g, and (c) 0.14 g of 16 000-*b*-7500 *via* spray-drying and calcination at 400 °C.

porosity. The specific surface area and the total pore volume are summarized in Table 1, including those prepared using 0.10 g of 16 000-*b*-7500. The analytical data, such as the SEM images with the N_2 adsorption–desorption isotherms, the TEM images, and the XRD patterns, are presented in Fig. 2–4, being almost analogous to those observed for the highly porous CeO_2 particles prepared using 0.10 g of 16 000-*b*-7500. By increasing the amount of 16 000-*b*-7500, the BET surface area and the total

Table 1 Porosities of PS-*b*-PEO-templated CeO_2 powders

PS-*b*-PEO		BET surface area/m^2 g^{-1}	Total pore volume/cm^3 g^{-1}
16 000-*b*-7500	0.10 g	177	0.36
	0.12 g	197	0.44
	0.14 g	202	0.46
59 000-*b*-31 000	0.10 g	169	0.36
	0.12 g	193	0.44
	0.14 g	184	0.28

pore volume gradually increased up to around 200 m^2 g^{-1} and around 0.46 cm^3 g^{-1}, respectively. Likewise, the powder samples were synthesized by spray-drying precursor solutions containing different amounts of 59 000-*b*-31 000 (0.10 g, 0.12 g, and 0.14 g) at 140 °C and then calcined at 400 °C. The SEM images with the N_2 adsorption–desorption isotherms, the TEM images, and the XRD patters are shown in Fig. 5–7, respectively. The resultant porosity (*e.g.*, specific surface area and total pore volume) are listed in Table 1. Although the analytical data seemed similar to those observed for the CeO_2 particles prepared using 16 000-*b*-7500, the BET surface area and the total pore volume were maximized to around 190 m^2 g^{-1} and around 0.44 cm^3 g^{-1} in the case of using 0.12 g of 59 000-*b*-31 000.

Highly porous CeO_2 powders (*e.g.*, specific surface area of 200 m^2 g^{-1} and total pore volume of 0.45 cm^3 g^{-1}, prepared using 16 000-*b*-7500 after calcination at 400 °C) were constructed by fine nanocrystals of CeO_2 (around 3 nm) through a thermal calcination, being much higher than those synthesized using different amphiphilic organic compounds (pore size of 5.5 nm, specific surface area of 125 m^2 g^{-1}, and total pore volume of 0.20 cm^3 g^{-1}, prepared using $EO_nPO_mEO_n$ after calcination at 500 °C; and pore size of 12 nm, specific surface area of 87 m^2 g^{-1}, and total pore volume of 0.12 cm^3 g^{-1}, prepared using KLE after calcination at 500 °C).[20,21] Even in the synthesis of pure CeO_2 using the laboratory-made 17 000-*b*-

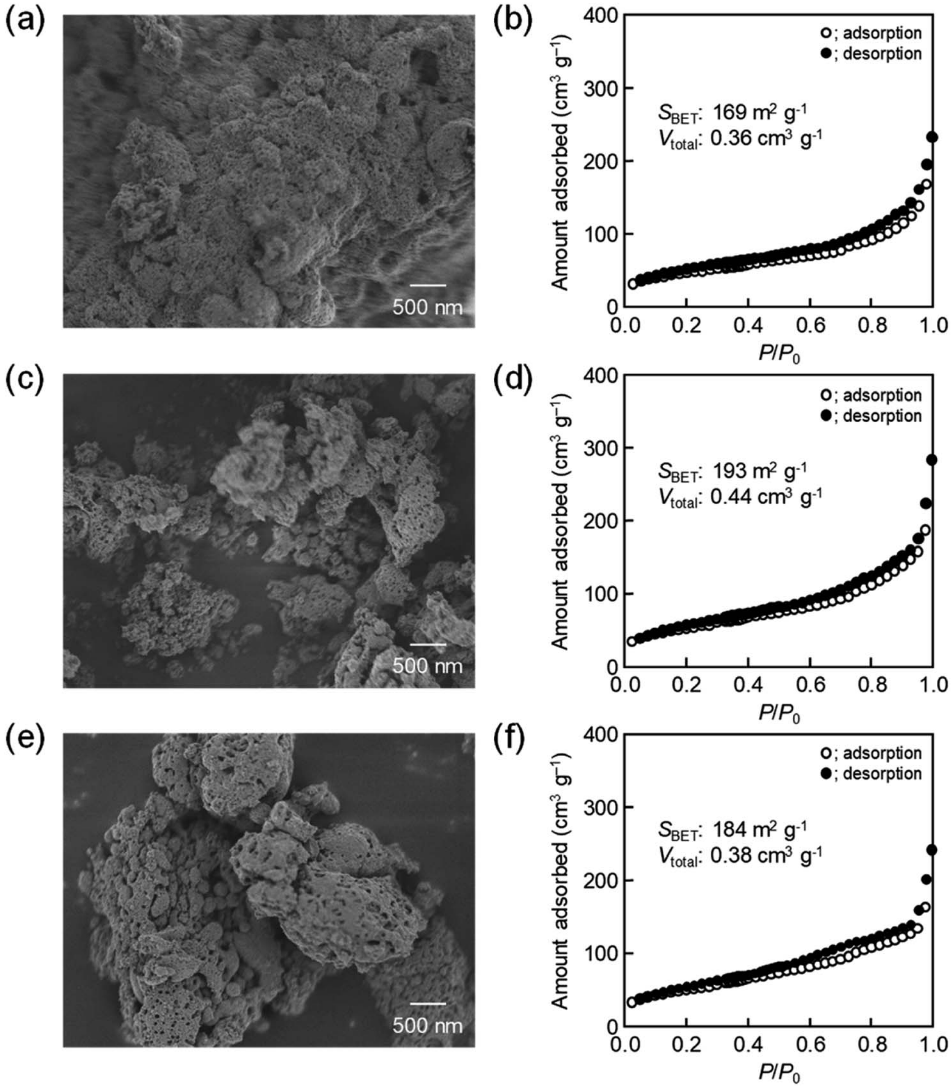

Fig. 5 SEM images of CeO_2 powders prepared using (a) 0.10 g, (c) 0.12 g, and (e) 0.14 g of 59 000-*b*-31 000 *via* spray-drying and calcination at 400 °C with (b, d and f) corresponding N_2 adsorption–desorption isotherms.

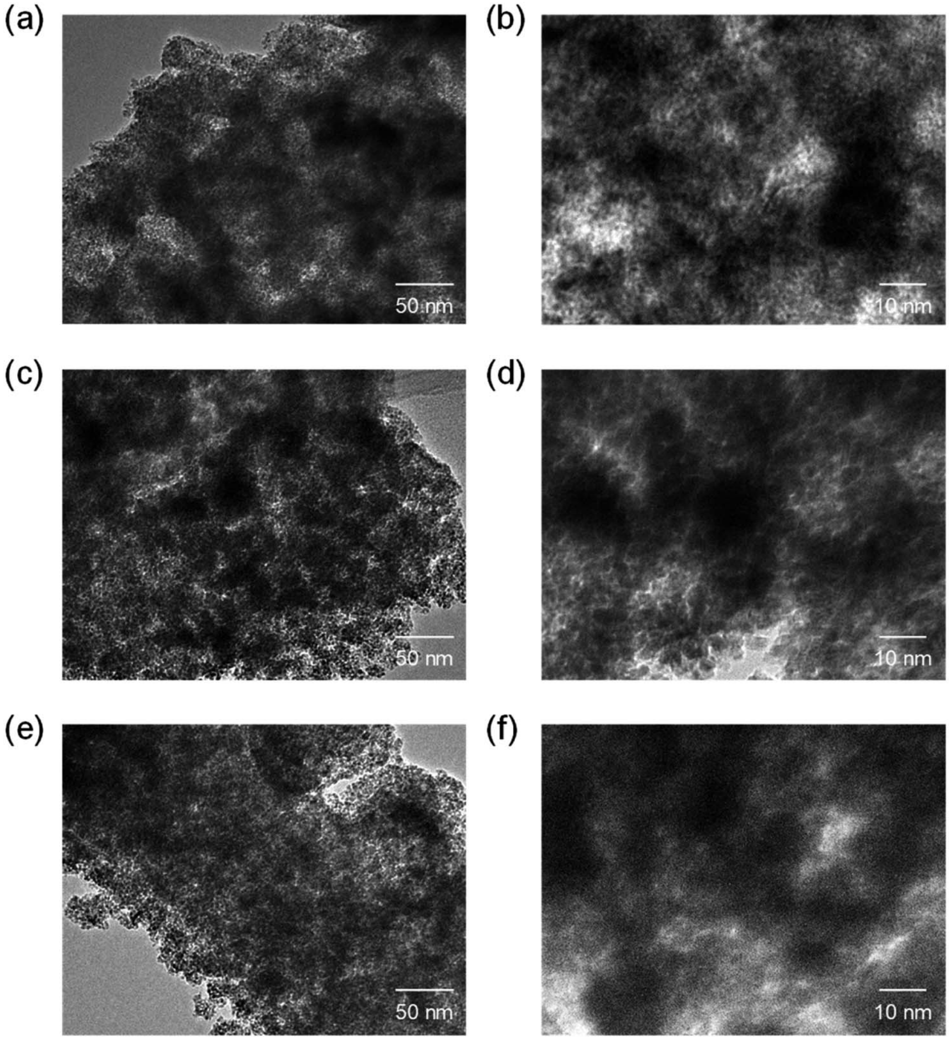

Fig. 6 TEM images of CeO_2 powders prepared using (a and b) 0.10 g, (c and d) 0.12 g, and (e and f) 0.14 g of 59 000-*b*-31 000 *via* spray-drying and calcination at 400 °C.

5000, the specific surface area and total pore volume were limited to 107 $m^2 g^{-1}$ and 0.32 $cm^3 g^{-1}$ with the formation of ~14 nm pores.[17] Such nano-sized CeO_2 crystallites are powerful materials for oxygen and charge storage[32,33] and useful for the design of metal-supported catalysts that depend on strong interaction with the surfaces of crystallized CeO_2 particles.[34–36] For example, a strong interaction of Pt to nanostructured CeO_2 surfaces is helpful for accelerating oxygen transfer from CeO_2 to

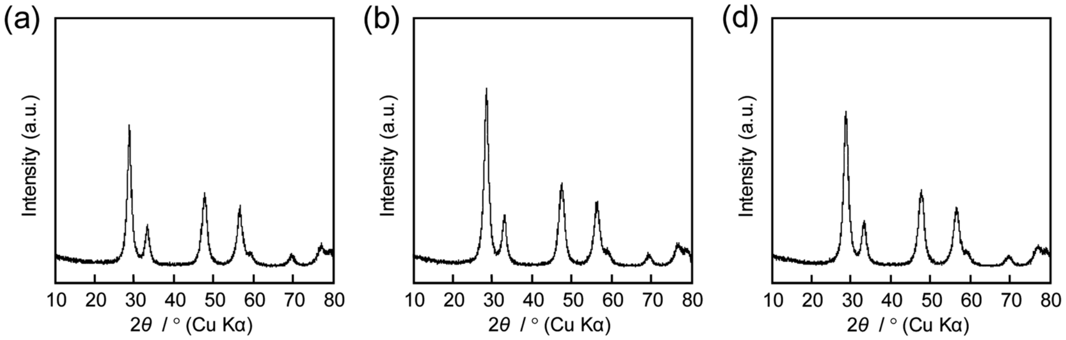

Fig. 7 XRD patterns of CeO_2 powders prepared using (a) 0.10 g, (b) 0.12 g, and (c) 0.14 g of 16 000-*b*-7500 *via* spray-drying and calcination at 400 °C.

Pt, leading to the formation of Pt–O species.[34] The size of CeO_2 nanocrystals (several nm order) is important for controlling the catalytic performance of atomically dispersed palladium (Pd).[36] The spray-pyrolysis technique is also very interesting for the design of single-atom catalysts over mesoporous metal oxides that are useful for low-temperature CO oxidation.[37–40] The resultant CeO_2 powders also possibly have potential for the design of metal-supported catalysts with an oxygen-storage capacity (OSC) for the purification of exhaust gases from automobiles.

4. Conclusion

A step-by-step but smooth optimization of the synthetic conditions was demonstrated as a rational approach for obtaining highly porous metal oxide powders through a spray-drying EISA process. As a typical example, a precursor solution, disclosed in the formative paper on the synthesis of a dried-up film-like bulk of CeO_2 with the formation of PS-*b*-PEO-templated mesopores during a slow evaporation of solvent(s) such as EtOH,[17] was utilized for screening the molecular structure of PS-*b*-PEO. After finding the molecular structure of PS-*b*-PEO that was most suitable for fabricating highly porous CeO_2 films by quick spin-coating (*e.g.*, 16 000-*b*-7500 and 59 000-*b*-31 000), the same precursor solution was spray-dried at an appropriate temperature (*e.g.*, 140 °C) for recovering high-quality porous CeO_2 powders, and the porosity was checked and/or increased by changing the amount of PS-*b*-PEO. In addition to our previous approach starting from the synthetic conditions optimized by a fast spin-coating process,[14] this extended approach to combine several EISA processes is promising for a smooth optimization of the synthetic conditions (*e.g.*, the chemical composition of the starting mixture and the molecular structure of the amphophilic organic compound) for obtaining highly porous metal oxides. Numerous papers concerning the dried-up powders and spin-coated films of metal oxides would be helpful for reproducing highly porous metal oxide powders by this temperature-controlled spray-drying process in the presence of a wide variety of amphiphilic organic compounds.[41,42]

Conflicts of interest

The author declares no competing financial interest.

Acknowledgements

This work has been mainly supported as one of the research projects (JPNP18016, commissioned by the New Energy and Industrial Technology Development Organization, NEDO) in the "Moonshot R&D program (Moonshot Goal 4: Realization of sustainable resource circulation to recover the global environment by 2050)".

References

1 C. T. Kresge, M. E. Leonowicz, W. J. Roth, J. C. Vartuli and J. S. Beck, *Nature*, 1992, **359**, 710–712.
2 Q. Huo, R. Leon, P. M. Petroff and G. D. Stucky, *Science*, 1995, **268**, 1324–1327.
3 D. Zhao, Q. Huo, J. Feng, B. F. Chmelka and G. D. Stucky, *J. Am. Chem. Soc.*, 1998, **120**, 6024–6036.
4 D. Zhao, J. Feng, Q. Huo, N. Melosh, G. H. Fredrickson, B. F. Chmelka and G. D. Stucky, *Science*, 1998, **279**, 548–552.
5 K.-W. Kim, B. Park, J. Kim, C. Jo and J. K. Kim, *J. Mater. Chem. A*, 2023, **11**, 7358–7386.
6 Q. Yuan, A.-X. Yin, C. Luo, L.-D. Sun, Y.-W. Zhang, W.-T. Duan, H.-C. Liu and C.-H. Yan, *J. Am. Chem. Soc.*, 2008, **130**, 3465–3472.
7 X. Xu, S. K. Megarajan, Y. Zhang and H. Jiang, *Chem. Mater.*, 2020, **32**, 3–26.
8 Y. Lu, R. Ganguli, C. A. Drewien, M. T. Anderson, C. J. Brinker, W. Gong, Y. Guo, H. Soyez, B. Dunn, M. H. Huang and J. I. Zink, *Nature*, 1997, **389**, 364–368.
9 D. Grosso, F. Cagnol, G. J. de A. A. Soler-Illia, E. L. Crepaldi, H. Amenitsch, A. Brunet-Bruneau, A. Bourgeois and C. Sanchez, *Adv. Funct. Mater.*, 2004, **14**, 309–322.
10 T. Kimura, *Chem. Rec.*, 2016, **16**, 445–457.
11 Y. Fu, H. Fan, A. Stump, T. L. Ward, T. Rieker and C. J. Brinker, *Nature*, 1999, **398**, 223–226.
12 C. Boissiere, L. Nicole, C. Gervais, F. Babonneau, M. Antonietti, H. Amenitsch, C. Sanchez and D. Grosso, *Chem. Mater.*, 2006, **18**, 5238–5243.
13 C.-K. Tsung, J. Fan, N. Zheng, Q. Shi, A. J. Forman, J. Wang and G. D. Stucky, *Angew. Chem., Int. Ed.*, 2008, **47**, 8682–8686.
14 H. Maruoka and T. Kimura, *Bull. Chem. Soc. Jpn.*, 2019, **92**, 1859–1866.
15 T. Kimura and H. Maruoka, *Chem. Commun.*, 2019, **55**, 10003–10006.
16 Md. I. Saidul, R. Wakabayashi and T. Kimura, *Dalton Trans.*, 2021, **50**, 7191–7197.
17 J. Ge, X. Yang, J. Luo, J. Ma, Y. Zou, J. Li, W. Luo, X. Cheng and Y. Deng, *Appl. Mater. Today*, 2019, **15**, 482–493.
18 T. Brezesinski, C. Erpen, K. Iimura and B. Smarsly, *Chem. Mater.*, 2005, **17**, 1683–1690.
19 K. Suzuki and A. K. Sinha, *J. Mater. Chem.*, 2007, **17**, 2547–2551.
20 J.-Y. Chane-Ching, F. Cobo, D. Aubert, H. G. Harvey, M. Airiau and A. Corma, *Chem.–Eur. J.*, 2005, **11**, 979–987.
21 A. S. Deshpande, N. Pinna, B. Smarsly, M. Antonietti and M. Niederberger, *Small*, 2005, **1**, 313–316.
22 M. Dubey, S. Wadhwa, A. Mathur and R. Kumar, *Appl. Surf. Sci. Adv.*, 2022, **12**, 100340.
23 C. Reitz, J. Haetge, C. Suchomski and T. Brezesinski, *Chem. Mater.*, 2013, **25**, 4633–4642.
24 Z. Lu, D. Rébiscoul, J. Causse, X. le Goff, N. Mollard and X. Deschanels, *J. Sol-Gel Sci. Technol.*, 2020, **94**, 174–185.
25 X. Yang, X. Cheng, H. Song, J. Ma, P. Pan, A. A. Elzatahry, J. Su and Y. Deng, *Adv. Healthcare Mater.*, 2018, **7**, 1800149.
26 X. Yang, X. Cheng, J. Ma, Y. Zou, W. Luo and Y. Deng, *Small*, 2019, **15**, 1903058.
27 Y. Zhang, R. Wakabayashi and T. Kimura, *Dalton Trans.*, 2023, **52**, 1543–1550.

28 Y. Deng, T. Yu, Y. Wan, Y. Shi, Y. Meng, D. Gu, L. Zhang, Y. Huang, C. Liu, X. Wu and D. Zhao, *J. Am. Chem. Soc.*, 2007, **129**, 1690–1697.
29 M. Lundberg, B. Skårman, F. Cesar and L. R. Wallenberg, *Microporous Mesoporous Mater.*, 2002, **54**, 97–103.
30 M. Lundberg, B. Skårman and L. R. Wallenberg, *Microporous Mesoporous Mater.*, 2004, **69**, 187–195.
31 A. Corma, P. Atienzar, H. García and J.-Y. Chane-Ching, *Nat. Mater.*, 2004, **3**, 394–397.
32 T. Brezesinski, J. Wang, R. Senter, K. Brezesinski, B. Dunn and S. H. Tolbert, *ACS Nano*, 2010, **4**, 967–977.
33 P. Hartmann, T. Brezesinski, J. Sann, A. Lotnyk, J.-P. Eufinger, L. Kienle and J. Janek, *ACS Nano*, 2013, **7**, 2999–3013.
34 J. A. Farmer and C. T. Campbell, *Science*, 2010, **329**, 933–936.
35 G. N. Vayssilov, Y. Lykhach, A. Migani, T. Staudt, G. P. Petrova, N. Tsud, T. Skála, A. Bruix, F. Illas, K. C. Prince, V. Matolín, K. M. Neyman and J. Libuda, *Nat. Mater.*, 2011, **10**, 310–315.
36 V. Muravev, A. Parastaev, Y. van den Bosch, B. Ligt, N. Claes, S. Bals, N. Kosinov and E. J. M. Hensen, *Science*, 2023, **380**, 1174–1178.
37 R. Li, Y. Yang, N. Sun and L. Kuai, *Chem.–Eur. J.*, 2019, **25**, 15586–15593.
38 Q. Tao, J. Song, N. Sun, Y. Ren, L. Xiang, S. Liu and L. Kuai, *Inorg. Chem.*, 2022, **61**, 11932–11938.
39 N. Sun, L. Xiang, B. Zhuge, E. Kan, N. Yu, L. Li and L. Kuai, *Inorg. Chem.*, 2023, **62**, 782–791.
40 L. Xiang, S. Wang and L. Kuai, *Microporous Mesoporous Mater.*, 2024, **363**, 112809.
41 J. Wei, Z. Sun, W. Luo, Y. Li, A. A. Elzatahry, A. M. Al-Enizi, Y. Deng and D. Zhao, *J. Am. Chem. Soc.*, 2017, **139**, 1706–1713.
42 Y. Zou, X. Zhou, J. Ma, X. Yang and Y. Deng, *Chem. Soc. Rev.*, 2020, **49**, 1173–1208.